SURFACE ALBEDO OBSERVATIONS AT GUSEV CRATER AND MERIDIANI PLANUM, MARS. M. S. Rice[1], J. F. Bell III[1], J. R. Johnson[2] and T. M. Hare[2]. [1]Department of Astronomy, Cornell University, Ithaca, New York, USA, mrice@astro.cornell.edu, [2]U.S. Geological Survey, Flagstaff, Arizona, USA.

Introduction: In this work we present the full suite of estimated bolometric albedo values measured to date by the Mars Exploration Rovers (MER) Spirit and Opportunity along their traverses in Gusev Crater and Meridiani Planum. We include albedo values of surface features (*e.g.* outcrops, dusty plains, aeolian bedforms, wheel tracks, light-toned soils, and crater walls) as well overall surface averages of all the 360° panoramic images acquired to date. We also present comparisons to estimated bolometric albedo values taken from the Mars Global Surveyor (MGS) Mars Orbiter Camera (MOC) along the Spirit and Opportunity traverses, and to the large-scale bolometric albedos of the sites as determined from the Viking Orbiter's Infrared Thermal Mapper (IRTM) and MGS's Thermal Emission Spectrometer (TES) [1]. These datasets will be a useful tool and benchmark for future investigations of albedo variations with time, as well as studies of aeolian processes, thermal inertia, and climate.

Accurate albedo measurements are essential to understanding the interactions between the martian surface and atmosphere. Since the early 19th century, ground-based observers have monitored regional variations in martian albedo (some originally interpreting them as evidence of vegetation growth/decay) [2]. While absolute calibration of early albedo maps was difficult, the observations still allowed for qualitative investigations of transient phenomena such as clouds, dust storms, and polar cap advance/recession [3,4]. Spacecraft investigations have since used measurements of the bolometric albedo (the fraction of total solar illumination reflected from the surface) to derive thermal inertia and evaluate solar heating and the global circulation of winds [*e.g.,* 5,6].

Albedo changes observed between the Mariner and Viking missions were used to monitor the movement of dust on Mars (high albedo regions are generally dust-covered, whereas lower albedo regions have exposed bedrock or duricrust) [7]. More recently, comparisons of Hubble Space Telescope (HST) and MGS measurements with Mariner and Viking images have shown that albedo has changed by 10% over more than one-third of the Martian surface in the past 30 years [8,9]. Such changes can have a significant effect on ground temperatures, and consequently can effect climatic parameters like thermal wind profiles and the radiative energy balance. Although surface albedo is a key parameter in general circulation models (GCMs), modelers have only recently begun to include temporally-varying albedo values [6,10,11]. Long-term, accurate albedo measurements will be key for future efforts in climate modeling as well as for studies of active surface processes.

To correctly interpret albedo variations on Mars, it is important to understand the relationship between the physical and *in situ* derived properties of the surface and the properties derived through remote sensing data. Estimated bolometric albedo images [12] taken by the Pancam instrument [13] during the MER missions have provided just such "ground-truth" data sets for comparison with orbital and telescopic data. Quantifying the reflectivity of characteristic surface units at the rover landing sites is also an important way to validate and cross-calibrate images taken by past, current, and future spacecraft [*e.g.,* 14].

Estimating Bolometric Albedo from Pancam Images: The scene reflectivity viewed by the Pancam instrument, usually around mid-sol, is estimated using near-simultaneous observations of the Pancam calibration target and its standard reflectance materials [12,13]. The reflectance products are called "IOF" (I over F) images, where IOF (also known as the "radiance factor" [15]), is defined as the ratio of the bidirectional reflectance of a surface to that of a normally illuminated, perfectly diffuse surface. Neglecting martian atmospheric effects, we can define:

$$IOF = \frac{I}{\pi F} \quad (1)$$

where I is the measured irradiance of the scene, and πF is the total solar irradiance at the top of the martian atmosphere at the time of each observation. Previous Mars orbiter and lander missions have used this same "*I/F*" as the radiance factor to compare with laboratory and telescopic reflectance measurements [12].

Dividing the Pancam IOF images by the cosine of the solar incidence angle at the time of each observation gives the parameter R* ("R-star") [12,16] (also known as the "reflectance factor" or "reflectance coefficient" [15]), which we use as an estimate of the Lambert bolometric albedo:

$$R^* = \frac{IOF}{\cos(i)} \quad (2)$$

This quantity is essentially the ratio of the reflectance of a surface to that of a perfectly diffuse surface under the same conditions. Images calibrated for R* allow for direct comparison between images taken at different times of day and are also partially "atmospherically corrected" because observations of the Pancam cali-

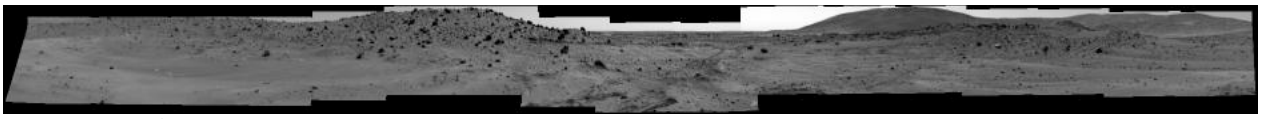

Figure 1. 360° Pancam albedo image taken by Spirit, sol 799, on its drive south from the Columbia Hills.

bration target also include the diffuse sky illumination component of the scene radiance [12].

We use R* calibrated images taken with Pancam's L1 (EMPTY) filter to estimate the bolometric albedo values presented in Tables 1 and 2. Because the broadband L1 filter (739 ± 338 nm) does not sample all solar visible wavelengths, R* is only an approximation of the bolometric albedo [12]. Uncertainties associate with this estimate must be generally small, however, given the overall agreement between our bolometric albedo estimates and previous orbital albedo observations of the landing sites [1,12,17,19].

Estimating the Average Surface Albedo: To calculate the average surface albedo of each scene, we average the R* values of all pixels below the horizon (neglecting the rover itself when applicable) in the cylindrically projected panoramic images (*e.g.,* Figs. 1,4). This method provides a good first-order estimate of the average scene albedo, but does not account for the differences in resolution and surface area between the near-field (mm/pixel) and the horizon (m/pixel).

Pancam Albedo Observations at Gusev Crater: As of sol 1150, the Spirit rover has acquired 11 panoramic images with Pancam's L1 filter for albedo measurements. The average surface albedos and standard deviations (variance among the selected pixels, not instrumental error) for each scene are listed in Table 1. All images are 360° panoramas except for those on sol 46 (180°) and sols 136-141 (250°). The portions of images compiled over multiple sols were acquired at roughly the same time of day for each sol. The majority of images taken by both rovers used 2x2 downsampling and 1 bit/pixel lossy compression.

The albedos measured by Spirit at Gusev Crater are moderately high for Mars [17,18]. Spirit's traverse

Table 1. Average albedo values and regional standard deviations measured by Pancam at Gusev Crater.

Sol(s)	Location	Surface Average	
		R*	σ
46	Drive to Bonneville Crater	0.21	0.04
136-141	Santa Anita, Gusev Plains	0.25	0.09
356	Columbia Hills	0.21	0.05
567-569	Climb up Husband Hill	0.19	0.04
627	Husband Hill Summit	0.22	0.05
656	East Basin, Husband Hill	0.16	0.03
720-725	Arad Bright Soil Target	0.14	0.03
799	Drive to Low Ridge	0.16	0.04
969	Low Ridge, Winter Haven 1	0.17	0.04
995	Low Ridge, Winter Haven 2	0.16	0.04
1026	Low Ridge, Winter Haven 3	0.22	0.06

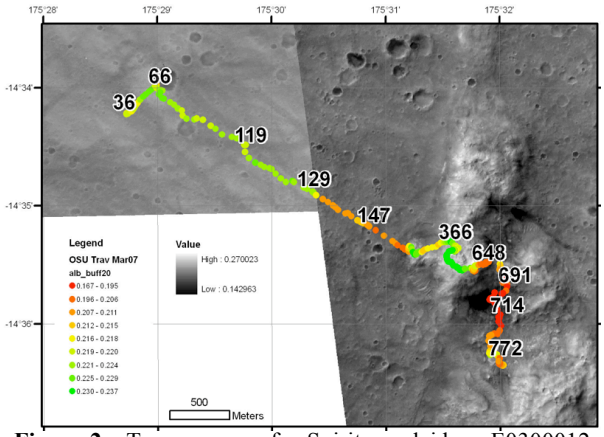

Figure 2. Traverse map for Spirit overlaid on E0300012 and R1303051 MOC images.

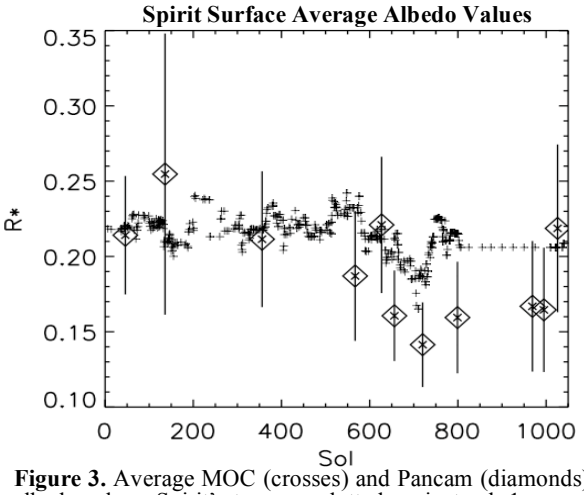

Figure 3. Average MOC (crosses) and Pancam (diamonds) albedos along Spirit's traverse plotted against sol. 1σ error bars correspond to the albedo variance within the selected scene, not to instrumental errors. Estimated uncertainties on the MOC-derived albedos are ± 20%.

towards the Columbia Hills is characterized by dust-devil tracks (Fig. 2), which have TES bolometric albedo values of ~0.19 within dark tracks and as high as ~0.26 within bright areas [1]. The range of average scene albedos measured by Pancam in the plains (sols 46 and 136-141) are comparable to the range derived from orbit, with high variations of R* within the image. No obvious change in average albedo was observed as Sprit moved from the plains into the hills, but average albedos were generally lower after the descent from the summit of Husband Hill. This could be the result of the increased areal abundance of low-albedo basaltic sand and rocks in the Southern Basin

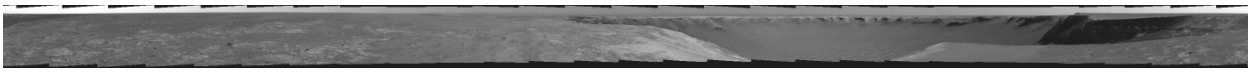

Figure 4. 360° Pancam albedo image taken by Opportunity, sol 1044, at the edge of Victoria Crater.

compared to the flanks and summit of Husband Hill.

Albedo values were also derived for individual surface units seen within each image, including dusty terrain, rocky terrain, dust devil tracks, aeolian bedforms, light-toned soils, duricrust, wheel tracks, rocks/boulders, and the "Home Plate" feature. Dusty terrain has consistently higher values than rocky terrain, and the highest albedo units (~0.46 at the "Tyrone" feature, sol 1026) are the patches of light-toned soils exposed by Spirit's wheels. Most aeolian bedforms have high albedo values (~0.24) except for the anomalously dark "El Dorado" dunes (~0.13) seen in several images near the southern base of Husband Hill. Although much of the surface appears to behave approximately Lambertian, some rocks and boulders exhibit strong specular glints and shadows (and thus high σ values), and our derived values may thus be poor estimates of these small-scale feature albedos.

Pancam Albedo Observations at Meridiani Planum: The Opportunity rover has acquired 31 panoramic images with Pancam's L1 filter for albedo measurements over the course of its traverse. Table 2 lists the average surface albedos and standard deviations for each scene. All images are 360° panoramas except for those on sol 68 (90°) and sol 309 (70°). The differences in average albedos calculated from the images taken in close succession (sols 409-411, 427-429, and 620-622) give an estimate of the errors inherent in our calibration scheme (<0.01).

The R* bolometric albedo estimates measured by Opportunity are consistently lower than those measured by Spirit, due to the dark, sand-rich, and relatively dust-free surfaces on the Meridiani plains; Opportunity represents the first landing in a low-albedo region of Mars [1]. Our albedo measurements are generally consistent with albedo values for the Opportunity landing site derived by IRTM (0.14 ± 0.06) and TES (0.12 ± 0.03) [1,18,19]. The highest albedo units measured along the traverse to date are the bright outcrop materials within Eagle Crater (0.25 ± 0.06). Although the traverse transitions from dark sand-dominated plains to light outcrop-abundant plains near the Erebus Rim, no obvious change in average surface albedo is observed across this boundary. We speculate that this is because most albedo images from the outcrop-abundant plains were not acquired while the rover was physically on light outcrops. Because of the unequal areal weighting of the near-field discussed earlier, the dark regions in front of the rover dominate the derived average albedos. Equal-area reprojection of the images may correct for this in future studies.

Individual surface units measured for bolometric albedo by Opportunity include sand- and hematitic-concretion-rich plains, rocky plains, light outcrop, aeolian bedforms, wheel tracks, airbag imprint marks, Eagle Crater outcrops, Victoria Crater outcrops, and Victoria Crater walls. For example, the outcrops within Eagle Crater have notably higher albedo (0.19 ± 0.03) than the average Meridiani plains.

Estimating Bolometric Albedo Along MER Traverse Paths from MOC Data: To calculate the MOC bolometric albedo values, we first radiometrically calibrated and projected the MOC images using ISIS software. For Spirit's traverse, MOC images E0300012 and R1303051 were used to cover the entire

Table 2. Average albedo values and standard deviations measured by Pancam at Meridiani Planum.

Sol	Location	Surface Average	
		R*	σ
22	Eagle Crater	0.18	0.06
68	Eagle Crater Rim, Plains	0.14	0.01
309	Endurance Crater, Plains	0.13	0.01
348	Heat Shield Rock, Plains	0.15	0.02
363	Plains Drive	0.14	0.02
374	Plains Drive	0.14	0.02
409	Plains Drive	0.16	0.02
411	Plains Drive	0.17	0.02
418	Plains Drive	0.17	0.02
427	Plains Drive	0.16	0.02
429	Plains Drive	0.16	0.02
435	Plains Drive	0.17	0.02
442	Plains Drive	0.16	0.02
454	Plains Drive	0.16	0.02
546	Plains Drive	0.17	0.04
572	Plains Drive	0.16	0.04
620	Erebus Rim	0.13	0.02
622	Erebus Rim	0.14	0.02
630	Erebus Rim	0.17	0.05
668	Erebus Rim	0.17	0.05
706	Erebus Rim	0.16	0.04
712	Erebus Rim	0.16	0.04
774	Plains Drive	0.17	0.03
790	Plains Drive	0.15	0.03
812	Plains Drive	0.15	0.03
856	Plains Drive	0.16	0.04
911	Victoria Dark Annulus	0.17	0.04
918	Victoria Dark Annulus	0.17	0.02
958	Victoria Crater, Cape Verde	0.11*	0.04
1015	Victoria Crater, Cape St. Mary	0.18	0.02
1044	Victoria Crater, Cabo Anomino	0.15	0.03

* Late afternoon observation; not included in Fig. 5

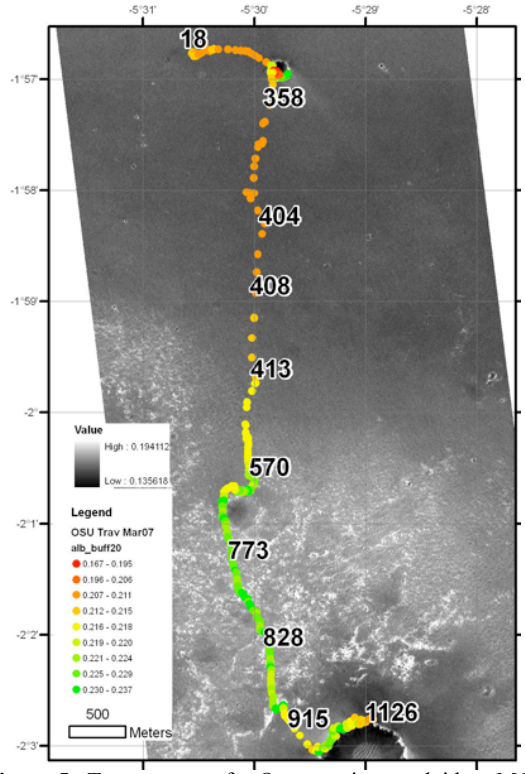

Figure 5. Traverse map for Opportunity overlaid on MOC image R140002.

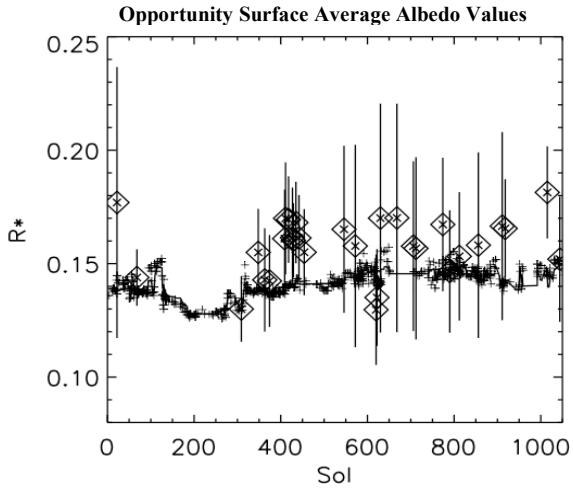

Figure 6. Average MOC (crosses) and Pancam (diamonds) albedos along Opportunity's traverse plotted against sol. 1σ error bars correspond to the albedo variance within the selected scene, not to instrumental errors. Estimated uncertainties on the MOC-derived albedos are ± 20%.

path. The Opportunity traverse is completely covered by the single MOC image R1400021. The traverse paths [20] along with the MOC images were ingested into a Geographic Information System (GIS). Slight spatial warping of the MOC images was required to warp the traverse points to the orbital images.

Comparison of Pancam and MOC albedos: The bolometric albedos derived from MOC and Pancam data along the rover traverses are plotted vs. sol in Figs. 3 and 6. The MOC-derived albedos shown were calculated from the single pixel representing each rover's position in the MOC images.

The Pancam-derived albedos follow the general trend of the MOC-derived values along the traverses. While the Pancam-derived albedos are generally higher than the MOC-derived albedos at Meridiani Planum, the MOC albedos fall within the variance of each Pancam scene with few exceptions, indicating that the atmosphere at the time of the MOC observation likely had a minimal effect on the measured surface radiance.

Conclusions and Future Work: We have derived surface bolometric albedo values from broadband (L1) Pancam panorama taken during the MER mission. The average Pancam albedo measurements at Gusev Crater (0.14-0.25) and at Meridiani Planum (0.13-0.18) are consistent with the bolometric albedos of the sites as determined from IRTM and TES. While albedo derived from MOC is typically lower than the ground-based rover measurements, they fall within the variances of the albedo at each scene.

Future studies will include comparisons of our derived albedos for surface averages and individual surface units to estimated bolometric albedos from the CTX and HiRISE instruments on the Mars Reconnaissance Orbiter mission. The CTX and HiRISE images will provide higher resolution data for more accurate comparisons of ground-based and orbital albedo values, and may allow us to identify temporal variations of albedo within each scene. These comparisons will provide a useful benchmark for a wide range of planetary science investigations.

References: [1] Golombek, M.P.*et al.* (2005) *Nature, 436,* 44-48. [2] de Vaucouleurs, G. (1954) *Physics of the Planet Mars,* Faber & Faber, London. [3] Pleskot, L.K. and E.D. Miner. (1981) *Icarus, 42,* 179-201. [4] Martin, L.J. *et al.*, (1992) in *Mars* (Kieffer H.H. *et al.*, eds.), U. Arizona Press, Tucson, 34-70. [5] Mellon, M.T. *et al* (2000) *Icarus, 148,* 437-455. [6] Haberle, R.M. *et al.* (1993) *JGR, 98,* 3093-3124. [7] Thomas, P. and J. Veverka (1979) *JGR, 84,* 8131-8146. [8] Bell, J.F. III *et al.* (1999) *Icarus, 138,* 25-35. [9]Geissler, P.E. (2005) *JGR, 110,* E02001. [10] Kahre, M.A. *et al.* (2005) *Icarus, 179,* 55-62. [11] Fenton, L.K. *et al.* (2007) *Nature, 446,* 646-649. [12] Bell III, J.F. *et al.* (2006) *JGR, 111,* E02S03, doi:10.1029/2005JE002444. [13] Bell, J.F., III, *et al.* (2003) *JGR, 108,* E12, doi:10.1029/2003JE002070. [14] McConnochie, T.H., *et al.* (2006) *JGR, 111,* E06018, doi:10.1029/2005JE002568. [15] Hapke, B. (1993), *Theroy of Reflectance and Emittance Spectroscopy*, Cambridge Univ. Press. [16] Reid, R.J. *et al.* (1999) *JGR, 104,* 8907-8926. [17] Bell, J.F., III, *et al.* (2004) *Science, 305,* 801-810. [18] Putzig, N.E. *et al.* (2005) *Icarus, 173,* 325-341. [19] Bell, J.F., III, *et al.* (2004) *Science, 306,* 1703-1709. [20] Li, R., *et al.*, (2004), *Photogramm. Eng. & Rem. Sens., 70(1),* 77–90.